Organic Electronics 15 (2014) 2367–2371

Contents lists available at ScienceDirect

Organic Electronics

journal homepage: www.elsevier.com/locate/orgel

Efficient organic near-infrared photodetectors based on lead phthalocyanine/C_{60} heterojunction

Xing Wang [a,b], Hongfei Li [c], Zisheng Su [a,*], Fang Fang [b], Guang Zhang [a], Junbo Wang [a], Bei Chu [a], Xuan Fang [b], Zhipeng Wei [b], Bin Li [a,*], Wenlian Li [a]

[a] State Key Laboratory of Luminescence and Applications, Changchun Institute of Optics, Fine Mechanics and Physics, Chinese Academy of Sciences, Changchun 130033, China
[b] Changchun University of Science and Technology, Changchun 130022, China
[c] School of Information and Electronics, Beijing Institute of Technology, Beijing 100081, China

ARTICLE INFO

Article history:
Received 5 June 2014
Received in revised form 3 July 2014
Accepted 5 July 2014
Available online 16 July 2014

Keywords:
Organic photodetector
Near-infrared
Small-molecule
Planar heterojunction

ABSTRACT

High efficiency organic small molecule near-infrared photodetectors (NIR-PDs) based on a lead phthalocyanine/C_{60} planar heterojunction are demonstrated. The NIR-PDs show a broad-band response that extends to 1100 nm. The performance of the NIR-PDs is improved by using CuI as anode buffer layer. The optimized NIR-PD exhibits a response peak at about 900 nm with external quantum efficiencies (EQEs) of 19.7% at zero bias and 35.1% at −6 V, which are higher than other small molecule NIR-PDs reported. Comparable EQEs of 18.0% at zero bias and 33.2% at −6 V are found in the NIR-PD by further using 4,7-diphenyl-1,10-phenanthroline as cathode buffer layer. Meanwhile, the dark current is significantly reduced, which results in a high detectivity of 2.34×10^{11} Jones at zero bias, which is among the highest detectivities reported for organic small-molecule NIR-PDs. Besides, the NIR-PDs show a reliable stability in ambient condition.

1. Introduction

Organic photodetectors (PDs) have been the subject of extensive research because of their large-area detection, wide selection of materials, and compatibility with flexible substrates [1–7]. Organic PDs for ultraviolet (UV) to visible wavelengths have been widely demonstrated. Near-infrared PDs (NIR-PDs) have tremendous potential in industrial and scientific applications, such as remote control, night vision, chemical/biological sensing, optical communication, and spectroscopic and medical instruments. Polymer NIR-PDs have attracted considerable interest in recent years [3,8–13]. Although high performance polymer NIR-PDs have been demonstrated, the difficult aspect of achieving even higher efficiency in polymer systems is the lack of precise control of their polydispersity index, regioregularity, molecular weight, etc. These parameters have to be taken into account in thin-film processing and have a strong correlation to the final detection performance. Materials with low molecular weight are an alternative to polymers for use in NIR-PDs. Binda and coworkers [14] reported a NIR-PD with an external quantum efficiency (EQE) of 15% at 700 nm based on a squaraine dye: [6,6]-phenyl-C61-butyric acid methylester (PCBM) blend. Wu et al. [15] fabricated a NIR-PD based on the charge transfer complexes formed in MoO_3 doped N,N′-di(naphthalene-1-yl)-N,N′-diphenyl-benzidine. We previously developed a NIR-PD based on copper-phthalocyanine (CuPc) and hexadecafluoro-copper-phthalocyanine, which realized an EQE of 9.22% at 808 nm at −8 V [16]. Although some small molecule NIR-PDs have been reported, many of their responses are only located shorter than 800 nm. Moreover, their EQE

* Corresponding authors.
E-mail addresses: suzs@ciomp.ac.cn (Z. Su), lib020@ciomp.ac.cn (B. Li).

http://dx.doi.org/10.1016/j.orgel.2014.07.008
1566-1199/

is low, which limits their application. Therefore it is desired to extend the response of small molecule NIR-PDs to longer wavelength and further increase their EQE. Zimmerman et al. [17] developed a NIR-PD based on a porphyrin-tape/C_{60} heterojunction that exhibited an EQE of 6.5% at 1350 nm. The EQE of this PD was enhanced to 13.5% at 1385 nm by adding 4,4′-bipyridyl into the porphyrin-tape/PCBM mixture [18]. Through a broad spectral response and a high EQE at the longer wavelength were demonstrated in these devices, the EQE at the region near 900 nm is low because of their lower absorption at this region.

Lead phthalocyanine (PbPc) is a shuttlecock-shaped molecule and has received attention recently in the field of organic photovoltaic devices because of its high absorption coefficient at the NIR wavelength region [19–26]. However, PbPc has not yet been used in NIR-PDs. PbPc films usually exhibit two absorption bands at NIR region. The band at 740 nm is related to the amorphous or monoclinic phases, while that at 900 nm is related to the triclinic phase. The formation of a triclinic phase is important to extend the absorption toward the NIR region. The crystal phase of a PbPc film is strongly related to the deposition method and conditions. PbPc with a triclinic phase can be obtained by controlling deposition conditions, such as the evaporation rate, the substrate temperature, and post-thermal annealing [19,20]. It can also be formed via deposition on a templating layer like zinc phthalocyanine [22], oxovanadium phthalocyanine [23], sexithiophene [23], para-sexiphenylene [23], CuPc [24], pentacene [24], or CuI [25,26]. In this study, PbPc is used as the NIR absorber to construct NIR-PDs. The fabricated NIR-PDs exhibit a broad-band response that extends to 1100 nm with a high response peak at 900 nm.

2. Experimental details

Devices were fabricated on patterned indium tin oxide (ITO) coated glass substrates with a sheet resistance of 15 Ω/sq. The substrates were routinely cleaned followed by UV-ozone treatment for 10 min. The devices have a structure of ITO/CuI/PbPc (60 nm)/C_{60} (60 nm)/Al (100 nm), here CuI, PbPc and C_{60} acted as the anode buffer layer, donor, and acceptor, respectively. The thickness of CuI varied from 0, 2, 4, to 6 nm (hereafter denoted as Device A, B, C, and D, respectively). The organic layers and Al cathode were sequentially deposited on the substrates by thermal evaporation in a vacuum chamber at a pressure of 5×10^{-4} Pa without breaking vacuum.

The dark currents of the devices were measured with a source meter (Keithley 2400). EQE spectra were obtained with a lock-in amplifier (Stanford SR803) under monochromatic illumination at a chopping frequency of 130 Hz by a chopper (Stanford SR540). Absorption spectra were recorded on a spectrophotometer (Lambda 950). X-ray diffraction (XRD) patterns were measured with a diffractometer (Rigaku D/Max-2500) using Cu Kα radiation (λ = 1.54056 Å). All measurements were carried out under ambient conditions.

3. Results and discussion

The EQE and detectivity (D^*) of a PD are sensitive to the thickness of the donor and/or acceptor layers in the device [7,24]. Although a thin organic active layer results in a high EQE [20,24], the resulting high dark current deteriorates the D^*. For example, the device ITO/PbPc (40 nm)/C_{60} (60 nm)/Al shows a high EQE of 15.6% at 900 nm but a low D^* of only 5.48×10^9 Jones at zero bias. Here, the thickness of PbPc and C_{60} was optimized at 60 nm each, which resulted in a PD with moderate EQE and high D^*. Fig. 1 shows the EQE spectrum of Devices A–D. Device A shows a broad-band response over the red to NIR wavelength region with two peaks at about 660 and 900 nm, and the EQE at 900 nm is 9.5%. Devices B–D exhibit EQE spectra with a similar shape to that of Device A. However, the EQE is dramatically enhanced, as listed in Table 1. Device C with a 4 nm thick CuI layer shows an EQE of 19.7% at 900 nm under zero bias, which is more than double that of Device A. This value is much higher than those of reported small molecule NIR-PDs at the same wavelength [14–16].

To understand the origin of the improved response of the devices with a CuI buffer layer, the properties of PbPc films on a CuI buffer layer were investigated. Fig. 2 shows the XRD patterns of the films of 60 nm PbPc films with different thickness of CuI on an ITO substrate, for reference XRD pattern of 4 nm CuI is also provided. PbPc with a triclinic phase is formed during the later stage of growth (>20 nm), whereas the monoclinic phase is formed during the initial growth (<10 nm) of a relatively thick film [24,25]. A weak diffraction peak at 2θ of about 6.9° is found in the PbPc film, which can be assigned to the (200) reflection plane of monoclinic phase [23]. This diffraction peak disappears in the PbPc films with a CuI buffer layer. Such a result is not shown by Shim et al. [26]. In contrast, a diffraction peak at 2θ of about 12.5° is found in the CuI/PbPc films. As there is no diffraction peak of CuI film in this region, this peak could be assigned to the $(11\bar{1})$ reflection plane of the triclinic phase or (320) of the monoclinic

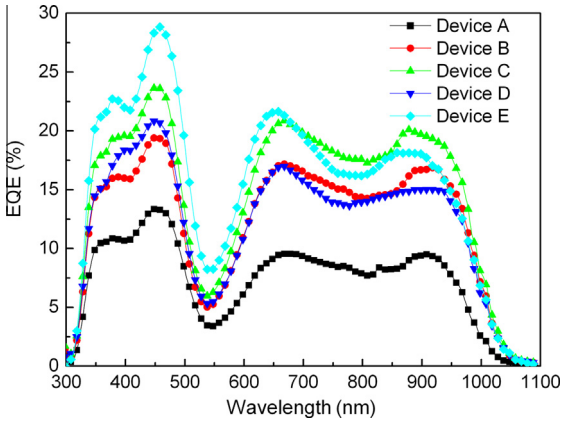

Fig. 1. EQE spectra of the devices ITO/CuI/PbPc(60 nm)/C_{60} (60 nm)/Al with CuI thickness of 0, 2, 4, and 6 nm (corresponding to Device A, B, C, and D), respectively, and ITO/CuI (4 nm)/PbPc(60 nm)/C_{60} (60 nm)/Bphen (10 nm)/Al (Device E) at zero bias.

Table 1
Performance of the NIR-PDs.

Device	EQE at 0 V (%)	EQE at −6 V (%)	D^* at 0 V (Jones)	D^* at −6 V (Jones)
A	9.5	20.6	6.01×10^{10}	4.12×10^{9}
B	16.7	31.8	6.23×10^{10}	1.54×10^{10}
C	19.7	35.1	6.60×10^{10}	3.19×10^{10}
D	15.1	30.9	6.38×10^{10}	3.13×10^{10}
E	18.0	33.2	2.34×10^{11}	6.63×10^{10}

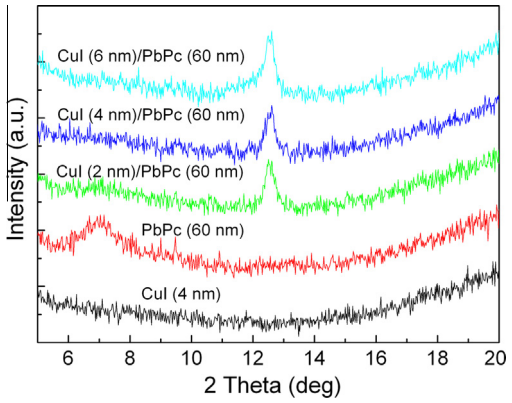

Fig. 2. XRD patterns of the films of 4 nm CuI and 60 nm PbPc with different thickness of CuI on an ITO substrate.

phase [26]. Because of their close peak positions, it is difficult to directly distinguish between the monoclinic and triclinic phases. These findings indicate that the CuI buffer layer may lead to the preferred growth of the PbPc film with the (3 2 0) orientation and/or the formation of the triclinic phase of PbPc.

Fig. 3 illustrates the absorption spectra of the films of 4 nm CuI and 60 nm PbPc with different thickness of CuI on a quartz substrate. The absorption spectrum of PbPc film without CuI shows a peak at about 730 nm with a shoulder at about 900 nm. The former results from the absorption of the amorphous or monoclinic phases, while the latter is from the triclinic phase [20]. This absorption

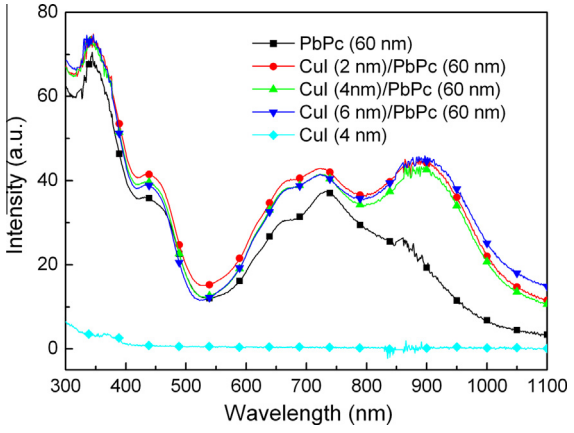

Fig. 3. Absorption spectra of the films of 4 nm CuI and 60 nm PbPc with different thickness of CuI on an ITO substrate.

profile differs from the EQE spectrum of Device A, which shows comparable intensity of these two peaks. The excitons are predominantly dissociated at the donor/accepter interface in a planar heterojunction photovoltaic device, so only the excitons that formation near this interface can efficiently dissociate into free charge carriers. We can deduce that the photocurrent generated in PbPc is mostly formed from excitons in the upper part of the PbPc film where there is a high content of triclinic phase. A similar result has also been found by Zhao et al. [24]. Interestingly, the absorption of the PbPc films increases upon inserting of a CuI buffer layer, especially at the region near 900 nm, which leads to a dramatic increase of absorption in the NIR wavelength region. Meanwhile, the thickness of the CuI layer has little effect on the absorption of the PbPc films. Thus the different EQE of the NIR-PDs with the thickness of CuI buffer layer cannot be attributed to their different absorption but to the hole extraction efficiency and which is optimized at 4 nm. The CuI film hardly absorbs in the NIR region, which indicates that the increase of NIR absorption can be attributed to the increased content of triclinic phase in the PbPc film [25,26]. Therefore the diffraction peak at 12.5° found in Fig. 2 may primary result from the formation of triclinic phase of PbPc when it is deposited on a CuI template layer. Such an increase of absorption is favorable to enhance the NIR response of PDs. It should be noted that the high energy peak was located at about 730 nm in the absorption spectra, and shifted to 660 nm in the EQE spectra. As only the excitons from the upper part of a PbPc film can efficiently dissociate into free charge carriers, the monoclinic phase of PbPc that dominates the lower part of the PbPc film has a small contribution to the photocurrent, which results in a dip at about 730 nm in the EQE spectra.

Another factor that determines the photocurrent of a device is the charge carrier collection efficiency. Cheng et al. [27] demonstrated that electron transfer will take place from ITO to CuI by investigating the UV and X-ray photoelectron spectroscopy, which induces a dipole layer formation at the ITO/CuI interface. This dipole layer raises the workfunction of the ITO surface by about 0.7 eV. According to these findings, the hole collection barrier of the PDs will be reduced by including a thin CuI buffer layer.

It has been reported that inserting a hole blocking layer between the organic active layer and cathode can enhance the response of the organic PDs [3]. This enhancement is attributed to reduced exciton quenching by the cathode and improved electron extraction efficiency. A hole blocking layer can also reduce the dark current of a device [28]. To validate these effects, another device with the structure of ITO/CuI (4 nm)/PbPc (60 nm)/C_{60} (60 nm)/

4,7-diphenyl-1,10-phenanthroline (Bphen, 10 nm)/Al (Device E) was fabricated. Device E did not exhibit an obvious increase of EQE in the NIR region (Fig. 1). This indicates that inserting a Bphen layer cannot improve exciton harvesting and the electron extraction efficiencies of our devices. Fig. 4 presents the EQE of Devices A, C, and E at 900 nm as a function of applied reverse voltage. The EQE of the devices increases with reverse voltage and reaches 20.6%, 35.1%, and 33.2% for Devices A, C, and E, respectively, at a reverse voltage of −6 V.

Fig. 5 compares the dark currents of Devices A, C, and E under reverse voltage. The dark current of the devices is reduced after the insertion of CuI and/or Bphen buffer layers, and this effect is more pronounced at higher reverse voltage. The dark current of Device E at −6 V is 0.041 mA/cm^2, which is two orders of magnitude lower than that of Device A. The highest occupied molecular orbital levels of C_{60} and Bphen are 6.2 and 6.4 eV, respectively [29]. This indicates that hole injection barrier from the Al cathode is increased by the presence of a Bphen buffer layer. Moreover, the shifts of the energy levels at the C_{60}/Bphen and Bphen/Al interfaces may also increase the hole injection barrier [30,31]. Combined with the fact that there is a 0.7 eV increase of the workfunction at the ITO/CuI interface [27], the reduced dark current at reverse voltage for the device with both Bphen and CuI layers can be attributed to the simultaneously increased hole and electron injection barriers at respective electrodes. It can be noted that the dark currents of these NIR-PDs are still higher than the state-of-the-art organic PDs [3,14,17]. The dark current of an organic photodiode is determined by the charge carriers injection from the contacts into the organic semiconductors, the charge carriers transport in the organic semiconductors, and the thermal generated charge carriers in the bulk and donor/acceptor interface [2]. Thus a lower dark current can be further expected by insertion of suitable self-assembling molecules or buffer layers between organic layer and metal electrode to suppress charge carriers injection [2,3,28,32].

The D^* of a PD can be calculated with the equation:

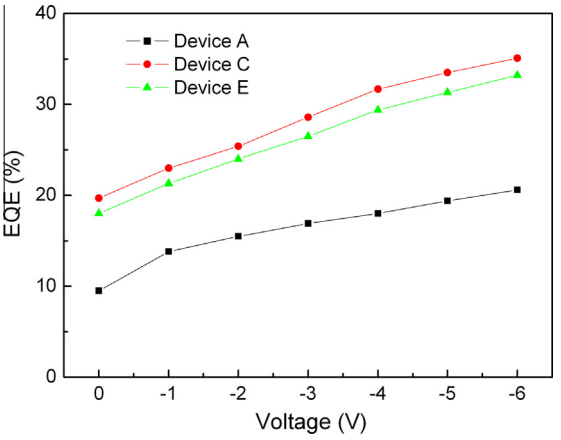

Fig. 4. EQE at 900 nm of ITO/PbPc(60 nm)/C_{60} (60 nm)/Al (Device A), ITO/CuI (4 nm)/PbPc(60 nm)/C_{60} (60 nm)/Al (Device C), and ITO/CuI (4 nm)/PbPc(60 nm)/C_{60} (60 nm)/Bphen (10 nm)/Al (Device E) as a function of applied reverse voltage.

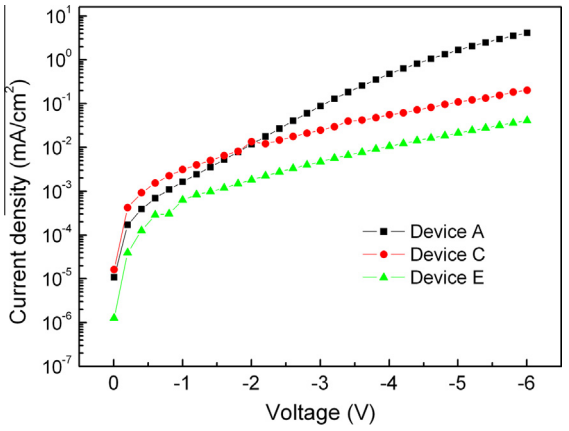

Fig. 5. Dark current of ITO/PbPc(60 nm)/C_{60} (60 nm)/Al (Device A), ITO/CuI (4 nm)/PbPc(60 nm)/C_{60} (60 nm)/Al (Device C), and ITO/CuI (4 nm)/PbPc(60 nm)/C_{60} (60 nm)/Bphen (10 nm)/Al (Device E).

$$D^* = R \cdot \sqrt{A}/S_N \tag{1}$$

where R is responsivity, A is the area, and S_N is the current spectral noise density. S_N^2 is the sum of all noise powers (e.g. thermal, shot, and excess noise). Under zero bias, the thermal noise dominates. In this situation, D^* can be calculated with the equation [33]:

$$D^* = R \cdot \sqrt{A \cdot R_D/(4k_BT)} \tag{2}$$

where R_D is the zero-bias differential resistance of the device, k_B is the Boltzmann constant, and T is the temperature. D^* of Devices A, C, and E at zero bias are 6.01×10^{10}, 6.60×10^{10}, and 2.34×10^{11} Jones, respectively, as listed in Table 1. Such D^* are comparable with those of other reported high performance small molecule NIR-PDs [14,17,18]. At high voltage, the shot noise from the dark current is the major contributor to the noise current. Then D^* can be expressed as [3]:

$$D^* = R/\sqrt{2qJ_d} \tag{3}$$

where q is absolute electron charge and J_d is dark current density. With increasing applied reverse voltage, D^* of the devices decreases, and it is only 4.12×10^9 Jones for Device A at −6 V. However, D^* of Device E reaches 6.63×10^{10} Jones because of it dramatically increased EQE and reduced dark current compared with those of Device A. As a result, D^* of Device E is more than one order of magnitude higher than that of Device A, which makes it more reliable for practical applications.

The stability is another important factor that limited the application of the NIR-PDs. Fig. 6 shows the dependence of EQE on storage time in ambient condition of Device E. It can be found that as the EQE falls to 50% of its initial intensity, the lifetime is about 190 h. This indicates that the NIR-PD has a reliable stability in ambient condition, and a longer lifetime can be expected with encapsulation.

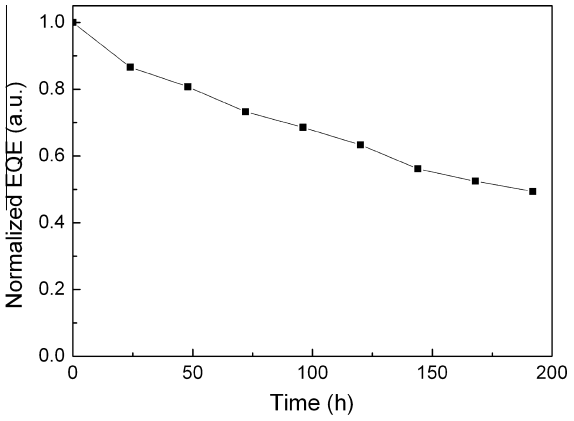

Fig. 6. Dependence of EQE on storage time in ambient condition of Device E ITO/CuI (4 nm)/PbPc(60 nm)/C_{60} (60 nm)/Bphen (10 nm)/Al.

4. Conclusion

In conclusion, a high efficiency organic NIR-PD based on a PbPc/C_{60} planar heterojunction was developed. The PD shows a broad-band response over the NIR wavelength region and its EQE at 900 nm reaches 9.5% at zero bias. The EQE of this device was further improved by using CuI and Bphen as anode and cathode buffer layers, respectively. The optimized device exhibits an EQE and D^* of 18.0% and 2.34×10^{11} Jones, respectively, at zero bias. When the applied reverse voltage was increased to −6 V, its EQE reached 33.2% with D^* of 6.63×10^{10} Jones. Such performance exceeds that reported for other small molecule NIR-PDs and is comparable to that of polymer counterparts. Besides, the NIR-PDs show a reliable stability in ambient condition. This work provides a route to design and fabricate simple high efficiency small molecule NIR-PDs.

Acknowledgements

This work was supported by the National Natural Science Foundation of China (61107082, 11004187, 61376062, 61376022, 61204065, and 61307045), the Science and Technology Development Plan of Jilin Province (20140101094JC), and the Research Fund for the Doctoral Program of Higher Education of China (20112216120005).

References

[1] H. Dong, H. Zhu, Q. Meng, X. Gong, W. Hu, Chem. Soc. Rev. 41 (2012) 1754.
[2] K.J. Baeg, M. Binda, D. Natali, M. Caironi, Y.Y. Noh, Adv. Mater. 25 (2013) 4267.
[3] X. Gong, M. Tong, Y. Xia, W. Cai, J.S. Moon, Y. Cao, G. Yu, C.L. Shieh, B. Nilsson, A.J. Heeger, Science 365 (2009) 1665.
[4] S.M. Menke, R. Pandey, R.J. Holmes, Appl. Phys. Lett. 101 (2012) 223301.
[5] X. Liu, H. Wang, T. Yang, W. Zhang, X. Gong, ACS Appl. Mater. Interfaces 4 (2012) 3701.
[6] Y. Sato, H. Kajii, Y. Ohmori, Org. Electron. 15 (2014) 1753.
[7] J. Qi, L. Ni, D. Yang, X. Zhou, W. Qiao, M. Li, D. Ma, Z. Wang, J. Mater. Chem. C 2 (2014) 2431.
[8] S.C.J. Meskers, J.K.J. van Duren, R.A.J. Janssen, F. Louwet, L. Groenendaal, Adv. Mater. 15 (2003) 613.
[9] Y. Yao, Y. Liang, V. Shrotriya, S. Xiao, L. Yu, Y. Yang, Adv. Mater. 19 (2007) 3979.
[10] E.C. Chen, S.R. Tseng, Y.C. Chao, H.F. Meng, C.F. Wang, W.C. Chen, C.S. Hsu, S.F. Horng, Synth. Metal. 161 (2011) 1618.
[11] G. Qian, J. Qi, J.A. Davey, J.S. Wright, Z.Y. Wang, Chem. Mater. 24 (2012) 2364.
[12] X. Hu, Y. Dong, F. Huang, X. Gong, Y. Cao, J. Phys. Chem. C 117 (2013) 6537.
[13] X. Liu, H. Wang, T. Yang, W. Zhang, I.F. Hsieh, S.Z.D. Cheng, X. Gong, Org. Electron. 13 (2012) 2929.
[14] M. Binda, A. Iacchetti, D. Natali, L. Beverina, M. Sassi, M. Sampietro, Appl. Phys. Lett. 98 (2011) 073303.
[15] S.H. Wu, M.F. Lo, Z.Y. Chen, T.W. Ng, X. Hu, H.W. Mo, C. Wu, W.L. Li, C.S. Lee, Phys. Status Solidi RRL 6 (2012) 129.
[16] J.B. Wang, W.L. Li, B. Chu, C.S. Lee, Z.S. Su, G. Zhang, S.H. Wu, F. Yan, Org. Electron. 12 (2011) 34.
[17] J.D. Zimmerman, V.V. Diev, K. Hanson, R.R. Lunt, E.K. Yu, M.E. Thompson, S.R. Forrest, Adv. Mater. 22 (2010) 2780.
[18] J.D. Zimmerman, E.K. Yu, V.V. Diev, K. Hanson, M.E. Thompson, S.R. Forrest, Org. Electron. 12 (2011) 869.
[19] A. Miyamoto, K. Nichogi, A. Taomoto, T. Nambu, M. Murakami, Thin Solid Films 256 (1995) 64.
[20] K. Vasseur, B.P. Rand, D. Cheyns, L. Froyen, P. Heremans, Chem. Mater. 23 (2011) 886.
[21] M. Hiramoto, K. Kitada, K. Iketaki, T. Kaji, Appl. Phys. Lett. 98 (2011) 023302.
[22] J. Dai, X. Jiang, H. Wang, D. Yan, Appl. Phys. Lett. 91 (2007) 253503.
[23] T. Sakurai, T. Ohashi, H. Kitazume, M. Kubota, T. Suemasu, K. Akimoto, Org. Electron. 12 (2011) 966.
[24] W. Zhao, J.P. Mudrick, Y. Zhang, W.T. Hammond, Y. Yang, J. Xue, Org. Electron. 13 (2012) 129.
[25] H.J. Kim, H.S. Shim, J.W. Kim, H.H. Lee, J.J. Kim, Appl. Phys. Lett. 100 (2012) 263303.
[26] H.S. Shim, H.J. Kim, J.W. Kim, S.Y. Kim, W.I. Jeong, T.M. Kim, J.J. Kim, J. Mater. Chem. 22 (2012) 9077.
[27] C.H. Cheng, J. Wang, G.T. Du, S.H. Shi, Z.J. Du, Z.Q. Fan, J.M. Bian, M.S. Wang, Appl. Phys. Lett. 97 (2010) 083305.
[28] P. Peumans, S.R. Forrest, Appl. Phys. Lett. 79 (2001) 126.
[29] M.Y. Chan, C.S. Lee, S.L. Lai, M.K. Fung, F.L. Wong, H.Y. Sun, K.M. Lau, S.T. Lee, J. Appl. Phys. 100 (2006) 094506.
[30] J.X. Tang, Y.C. Zhou, Z.T. Liu, C.S. Lee, S.T. Lee, Appl. Phys. Lett. 93 (2008) 043512.
[31] T. Sakurai, S. Toyoshima, H. Kitazume, S. Masuda, H. Kato, K. Akimoto, J. Appl. Phys. 107 (2010) 043707.
[32] H.L. Yip, A.K.Y. Jen, Energy Environ. Sci. 5 (2012) 5994.
[33] M.S. Arnold, J.D. Zimmerman, C.K. Renshaw, X. Xu, R.R. Lunt, C.M. Austin, S.R. Forrest, Nano Lett. 9 (2009) 3354.